Palaeogeography, Palaeoclimatology, Palaeoecology 510 (2018) 6–14

Contents lists available at ScienceDirect

Palaeogeography, Palaeoclimatology, Palaeoecology

journal homepage: www.elsevier.com/locate/palaeo

What enhanced the aridity in Eocene Asian inland: Global cooling or early Tibetan Plateau uplift?

Xiangyu Li[a], Ran Zhang[a], Zhongshi Zhang[b,c,d,*], Qing Yan[c]

[a] Climate Change Research Center, Chinese Academy of Sciences, Beijing 100029, China
[b] Department of Atmospheric Science, School of Environmental Studies, China University of Geosciences (Wuhan), Wuhan 430074, China
[c] Nansen-Zhu International Research Centre, Institute of Atmospheric Physics, Chinese Academy of Sciences, Beijing 100029, China
[d] Uni Research Climate, Uni Research and Bjerknes Centre for Climate Research, Bergen 5007, Norway

ARTICLE INFO

Keywords:
Aridification
CO_2 decrease
Land–sea distribution
India–Asia collision
Paleoclimate modeling

ABSTRACT

Geological evidence shows that the Asian inland environment experienced enhanced aridity from the Early to the Late Eocene. This enhanced Eocene aridity in the Asian inland was related to combined impacts from global cooling, topographic uplift and land–sea reorganization. However, the primary cause of the enhanced Eocene aridity in this region is still under debate and varies between global cooling and early Tibetan Plateau uplift. To distinguish between the importance of these factors, we evaluate the climatic impacts of these factors from a modeling point of view. Consistent with geological evidence, our simulations support the observed enhanced Eocene aridity in the Asian inland. Both global cooling (induced by atmospheric CO_2 decrease) and topographic uplift contributed to intensified Asian inland aridity, while land–sea redistribution did not. The uplift of the central Tibetan Plateau during the early stage of the India–Asia collision is emphasized more to be responsible for the long-term Asian inland aridification during the Eocene, playing at least an equally important role as the global cooling induced by decrease in atmospheric CO_2.

1. Introduction

During the Cenozoic, aridification of the Asian inland developed with a prolonged climate change from a relatively warmer and wetter climate to a cooler and drier climate (Liu, 1985; Rea et al., 1998; An et al., 2001; Guo et al., 2002; Dupont-Nivet et al., 2007). Previous studies have demonstrated intensified Asian inland aridity during the Late Miocene (Fang et al., 1997; Liu et al., 1998; Sun et al., 1998; Ding et al., 1999; Zhuang et al., 2011; Sun et al., 2015), the Early Miocene (Guo et al., 2002; Guo et al., 2008), the Late Oligocene (Sun et al., 2010; Qiang et al., 2011; Tang et al., 2011; Y. Zhang et al., 2014; Zheng et al., 2015), and Eocene-Oligocene transition (Sun and Windley, 2015).

Recent research has pushed the earliest Cenozoic Asian inland aridification back to the Eocene. Palynological and palaeoenvironmental evidence show that Asian inland aridity intensified from the Early to the Late Eocene (Sun and Wang, 2005; Song et al., 2013; Bosboom et al., 2014b; Fang et al., 2015; Miao et al., 2016). In the Xining–Minhe Basin of western China, *Ephedripites*, a representative pollen type of arid climate, occurred sporadically in the Early Eocene but increased sharply to 37.3% during the Middle and Late Eocene (Sun and Wang, 2005). Pollen records from the Xining Basin show an increased percentage of desert-steppe vegetation in the pollen assemblage at ~40 Ma (Bosboom et al., 2014b; Fig. 1A and B). The degree of chemical weathering in the Dahonggou section, northeast of the Qaidam Basin, decreased markedly at ~40.5 Ma, together with a gradual decrease in broad-leaved trees and an increase in xerophilous elements (Song et al., 2013). Furthermore, it has been identified that arid climates in the Late Eocene covered a large region in northwestern China, characterized by similar arid palynological assemblages in the Hoh Xil, Qaidam, Xining, Jiuquan, Hetao and Tu-ha basins (Fu et al., 1994; Jin, 1996; Miao et al., 2008; Miao et al., 2016).

The enhanced Eocene Asian inland aridity is usually attributed to global cooling (Bosboom et al., 2014b; Fang et al., 2015), topographic uplift (Graham et al., 2005; Wang et al., 2008; Song et al., 2013), and land–sea redistribution (e.g., Abels et al., 2011; Bosboom et al., 2011, 2014a). These factors are supposed to have reduced the moisture supply to the Asian interior, enhancing aridity there (e.g., Dupont-Nivet et al., 2007; Abels et al., 2011; Bosboom et al., 2011, 2014a).

However, it is still difficult to distinguish the importance of these factors. How and to what extent these factors impacted the Eocene Asian inland enhanced aridity are still questions open to debate.

* Corresponding author at: Department of Atmospheric Science, School of Environmental Studies, China University of Geosciences (Wuhan), Wuhan 430074, China.
E-mail address: Zhongshi.Zhang@uni.no (Z. Zhang).

https://doi.org/10.1016/j.palaeo.2017.10.029
Received 26 June 2017; Received in revised form 28 October 2017; Accepted 28 October 2017
Available online 31 October 2017
0031-0182/ © 2017 Published by Elsevier B.V.

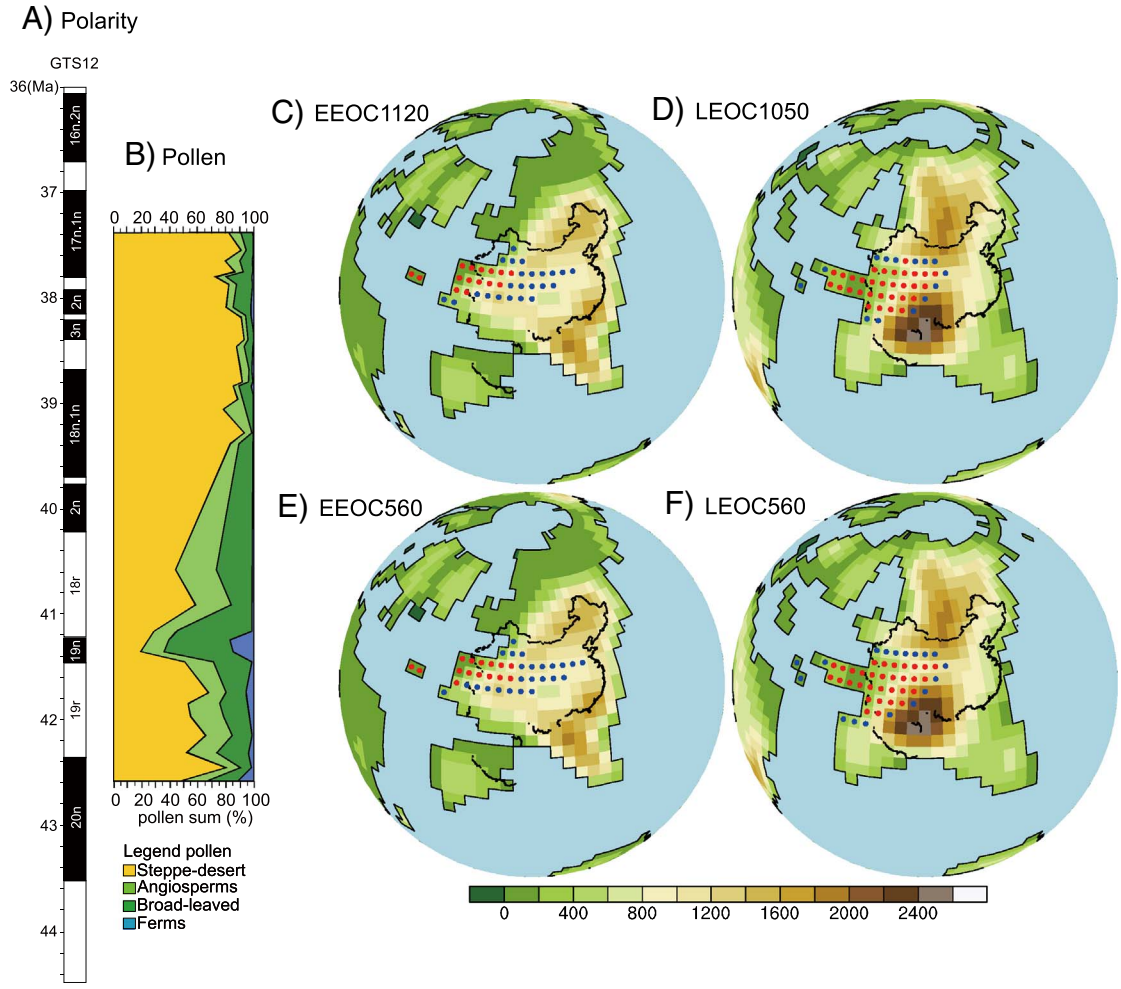

Fig. 1. Permanent enhanced aridification during the Eocene epoch in central Asian explored by pollen records and model simulations. Against geological time (A), we show the composite pollen record from Xining Basin (B) in the two left panels (Bosboom et al., 2014b). In the four right panels the precipitation patterns are simulated for the Early Eocene (C and E) and the Late Eocene (D and F) epochs. We carry out experiments with both decreased CO_2 concentration scenario (1120 ppmv in C and 1050 ppmv in D) and fixed CO_2 concentration scenario (560 ppmv in E and F) from the Early Eocene to the Late Eocene. The colored shading shows the reconstructed elevations (units: m). The dark blue dots indicate Asian regions with annual precipitation between 200 and 400 mm, and the red dots indicate Asian regions with annual precipitation less than 200 mm. (For interpretation of the references to colour in this figure legend, the reader is referred to the web version of this article.)

Recently, it was highlighted that global climate cooling from greenhouse to icehouse conditions seemed to be the primary driver of the enhanced aridity during the Eocene (Bosboom et al., 2014b; Fang et al., 2015). However, the early topographic growth of the Himalayan-Tibetan Plateau may have also contributed to the reorganization of the climate farther north in central Asia during the Eocene (Graham et al., 2005; Wang et al., 2008; Song et al., 2013). In the early stages of the convergence of India and Asia, the central Tibetan Plateau is thought to have been comparable to its present day height by the Eocene (Graham et al., 2005; Mulch and Chamberlain, 2006; Rowley and Currie, 2006; Wang et al., 2008; Polissar et al., 2009). This high Tibetan Plateau would have enhanced aridity in the Asian inland (e.g., Ruddiman and Kutzbach, 1991; Zhang et al., 2015). Moreover, the land–sea redistribution in the Eocene could modify the local moisture transport in the Asian inland and could influence the evolution of regional aridity.

Comprehensive understanding of how tectonics and global climate impact the aridification of the Asian inland is limited in part by the difficulties in distinguishing their importance based only on geological reconstruction. In this study, we carry out climate simulations to distinguish the importance of these factors on the enhanced Eocene Asian inland aridity. The paper is organized as follows. Section 2 describes the model and experiment design. Section 3 presents simulation results. Then we discuss the uncertainties on atmospheric CO_2 concentration and topography (Section 4.1) and the implication for intensified Eocene Asian aridity (Section 4.2), and finally provide a summary.

2. Model and experimental design

2.1. Model introduction

The coupled atmosphere-ocean simulation model used here is the low-resolution version of the Norwegian Earth System Model (NorESM-L). The NorESM-L is an Earth system model developed for paleoclimate simulations at the Bjerknes Centre for Climate Research. It uses the structure of the Community Earth System Model (CESM) from the National Center for Atmospheric Research (NCAR). However, the ocean component is replaced by the Miami Isopycnic Coordinate Ocean Model (MICOM), and the atmosphere component is optionally modified with an advanced chemistry–aerosol–cloud–radiation interaction scheme. Detailed model introductions can be found in Z.S. Zhang et al. (2012) and Bentsen et al. (2013). In the NorESM-L, the atmosphere component is the spectral Community Atmosphere Model Version 4 (CAM4), with a resolution of T31 (~3.75°) in the horizontal and 26 levels in the vertical. The ocean component resolution is g37 (~3°) in the horizontal, and 32 layers in the vertical. The model well simulates pre-industrial climate and paleoclimate (Z. Zhang et al., 2012, 2013, 2014; Bentsen

et al., 2013).

To further investigate the climate effects of these factors, we use the higher-resolution CAM4 to carry out sensitivity experiments. The higher-resolution CAM4, 0.9° latitude by 1.25° longitude grid and 26 vertical levels, employs a finite-volume dynamical core for horizontal discretization (Lin and Rood, 1997; Lin, 2004) and Lagrangian with a conservative remapping for vertical discretization. The 0.9° latitude by 1.25° longitude grid is the default resolution for most CAM4 applications (Neale et al., 2013). With a better resolved topography, the higher-resolution CAM4 provides better simulation for precipitation (Gent et al., 2010). The CAM4 reasonably simulates the large-scale Asian circulation (R. Zhang et al., 2012).

2.2. Boundary conditions and experimental design

2.2.1. Coupled experiments

Based on the global paleogeography map database by Scotese (2001) for ~50 Ma and ~40 Ma, we create the boundary conditions for the Early and Late Eocene, following the procedures outlined by Z. Zhang et al. (2011, 2014). We configure land–sea distributions and relief topography based on referring datasets of mountains and coastlines. Based on the age-depth relationships built by Bice et al. (1998), we establish bathymetric conditions following the method presented by Bice et al. (1998).

In the Early Eocene, high mountains located in southern China are set to less than 2000 m above sea level (asl), and the Tibetan Plateau height ranges from 800 to 1300 m asl (Fig. 1C and E). In the late Eocene, we close the West Siberian Seaway and the Tibetan Plateau is set to 1600–2600 m asl with a greater area. The relief topography in southern China is reduced to less than 800 m asl while the Mongolian Plateau is as high as 2000 m asl with a greater area.

With these land–sea distribution and topography conditions, we carry out four coupled experiments (Table 1). These experiments are divided into two groups. In the first group, we use different CO_2 levels, 1120 ppm by volume (ppmv hereafter) for EEOC1120 experiment, and 1050 ppmv for LEOC1050 experiment. In the second group, we use fixed CO_2 levels, 560 ppmv for experiments EEOC560 and LEOC560. Except for atmospheric CO_2 concentration, all other trace gases and aerosols are specified to present conditions. Other boundary condition in the Early and Late Eocene coupled experiments are kept identical, including idealized vegetation conditions with forest between 30°N and 30°S and shrub/grass outside this latitude band. The coupled experiments could simulate out the see surface temperature, which is the necessary boundary conditions for the following atmosphere-only sensitivity simulations. All coupled experiments run for 2200 yr. The climatological mean of the last 200 yr are used here.

Table 1
Boundary conditions and experimental design.

NorESM-L coupled experiments			
Experiments	Land-sea	Topography	CO_2 (ppmv)
EEOC1120	50 Ma	50 Ma	1120
LEOC1050	40 Ma	40 Ma	1050
EEOC560	50 Ma	50 Ma	560
LEOC560	40 Ma	40 Ma	560

CAM4 high-resolution experiments				
Experiments	Land-sea	Topography	SST	CO_2 (ppmv)
EE560	50 Ma	50 Ma	EEOC560	560
LE560	40 Ma	40 Ma	LEOC560	560
EE560Flat	50 Ma	FLAT	EEOC560	560
LE560Flat	40 Ma	FLAT	LEOC560	560
EE1120Flat	50 Ma	FLAT	EEOC1120	1120
LE1050Flat	40 Ma	FLAT	LEOC1050	1050

2.2.2. Sensitivity experiments

To distinguish the impacts of topography, land–sea redistribution and global cooling induced by atmospheric CO_2 decrease, we design six sensitivity experiments (Table 1). In these six experiments, the difference between LE560Flat and EE560Flat shows the climate impact of the land–sea redistribution, including the impact of sea surface temperature change due to land–sea redistribution. The difference between LE1050Flat and EE1120Flat includes the climate impacts of two factors, the global cooling induced by atmospheric CO_2 decrease and the land–sea redistribution. Thus, the difference ((LE1050Flat − EE1120Flat) − (LE560-Flat − EE560Flat)) shows the climate impact of the global cooling induced by atmospheric CO_2 decrease. Finally, the difference ((LE560 − LE560Flat) − (EE560 − EE560Flat)) shows the climate impact of topography. In total, the integration of ((LE560 − LE560 Flat) − (EE560 − EE560Flat) + (LE1050Flat − EE1120Flat)) shows the total climate impact of these three factors. In these six experiments, other boundary conditions are kept identical, including idealized vegetation conditions with only shrub on land, and present solar constant and orbital parameters. All CAM4 experiments run for 25 yr. The average of the last 20 yr is analyzed here.

In the EE560 and LE560 experiments, we use high-resolution reconstructed topography. In experiment EE560, the relief topography in southern China ranges from 1600 to 2200 m asl, and the average southern Tibetan Plateau is specified at 1300 m asl, with heights varying from 800 to 1800 m asl (see Supplementary Fig. 1). In experiment LE560, the Tibetan Plateau ranges from 2200 to 2800 m asl. The topography in southern China is reduced to less than 1000 m asl high and the Mongolian Plateau is approximately 2000 m asl.

3. Results

3.1. Evolution of precipitation

The simulated annual precipitation decreased in the Late Eocene experiments compared to that in the Early Eocene experiments (Fig. 1C–F). Here, we use 200 mm and 400 mm isohyetal lines of annual precipitation to outline the Asian arid and semi-arid regions. In the EEOC1120 experiment, the zonal-like arid and semi-arid bands extend from west to east, and the arid region covers a small part of western China. In the LEOC1050 experiment, the semi-arid region withdraws westward and most of western China is dominated by arid climate with an annual precipitation less than 200 mm. In the red rectangle region (Fig. 2), the annual averaged precipitation decreases by 107 mm in the LEOC1050 compared to the EEOC1120 (Fig. 3A), by 76 mm in the LEOC560 compared to the EEOC560 (Fig. 3B), and by 107 mm in the LE560 compared to the EE560 (Fig. 3C).

In the sensitivity experiments, the regional annual precipitation decreases under the climate impacts of topographic uplift and global cooling induced by atmospheric CO_2 decrease. In contrast, the regional annual precipitation increases under the climate impact of the land–sea redistribution (Fig. 3G and H).

The topography causes the Asian inland annual precipitation to decrease by 88 mm under the Early Eocene boundary condition (EE560 − EE560Flat). Under the Late Eocene boundary condition, the topography leads to the Asian inland annual precipitation decreasing by 368 mm (LE560 − LE560Flat). In total, the topography change causes an annual precipitation reduction of 280 mm in the Late Eocene experiments when compared to the Early Eocene experiments ((LE560 − LE560Flat) − (EE560 − EE560Flat)) (Fig. 3G and H). The decrease in the atmospheric CO_2 level, from 1120 ppmv to 1050 ppmv, causes the Asian inland annual precipitation to decrease by 161 mm in the Late Eocene experiment relative to the Early Eocene experiment ((LE1050Flat − EE1120Flat) − (LE560Flat − EE560Flat)) (Fig. 3G). The land–sea redistribution increases the Asian inland annual

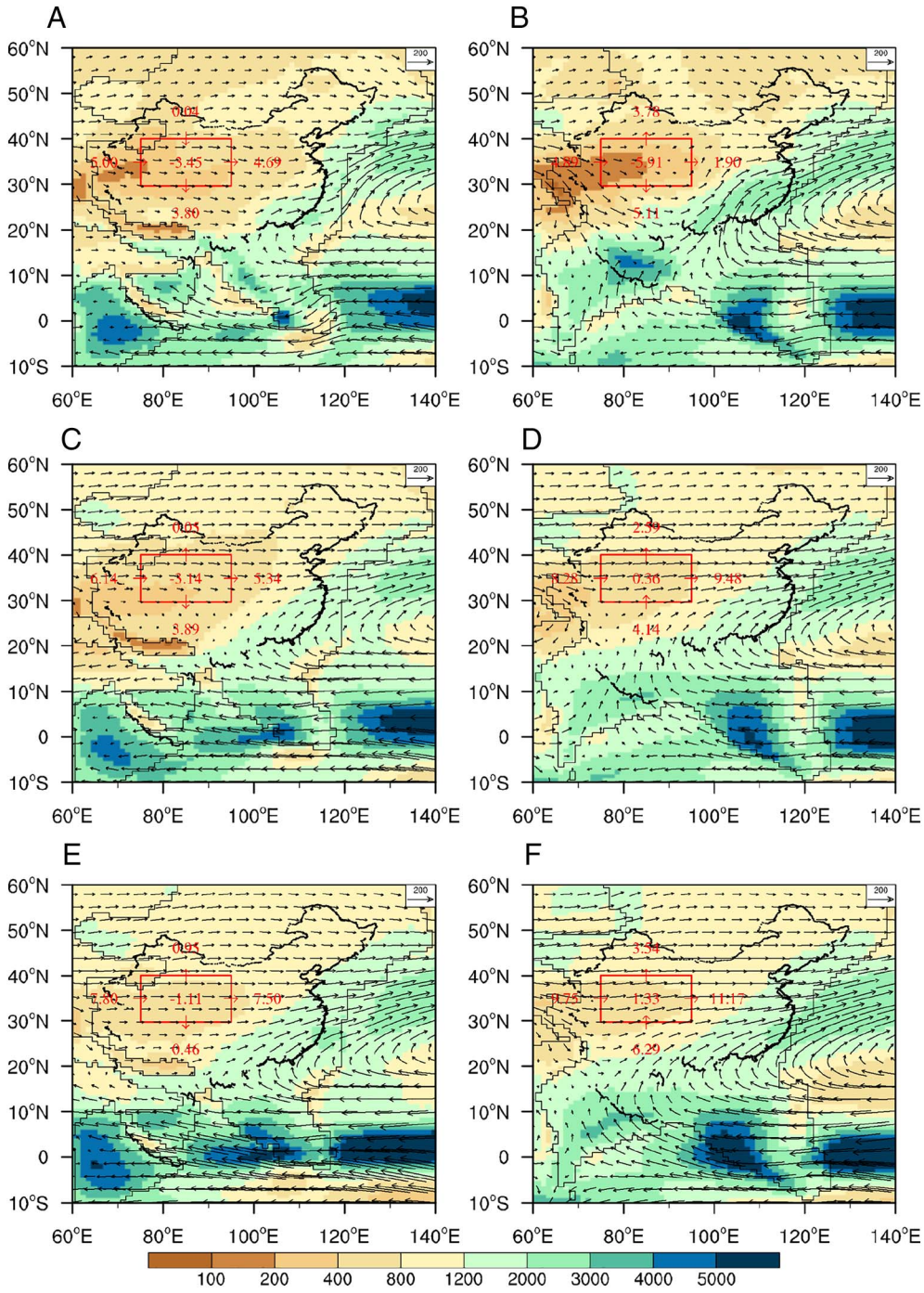

Fig. 2. Annual precipitation (shading, units: mm) and vertically integrated water vapor flux (arrow, units: kg m^{-1} s^{-1}) in the Early Eocene experiments (left panels) and in the Late Eocene experiments (right panels): EE560 vs. LE560 (in A and B), EE560Flat vs. LE560Flat (in C and D), and EE1120Flat vs. LE1050Flat (in E and F). The red rectangle outlines the focused region over the Asian inland (30°–40° N, 75°–95° E). (For interpretation of the references to colour in this figure legend, the reader is referred to the web version of this article.)

precipitation by 174 mm (LE560Flat − EE560Flat) (Fig. 3G and H). The total climate impact of these three factors induces an annual precipitation reduction of 267 mm in the Late Eocene experiments when compared to the Early Eocene experiments (Fig. 3G).

3.2. Underlying mechanism of forcing factors

To further understand the change in the precipitation, we analyze the moisture transport in the Asian inland. In the EEOC1120 experiment, moisture is transported into the red rectangle region by westerlies from the west boundary and northerlies from the north boundary, and out of the region by westerlies from the east boundary and by southerlies from the south boundary. The regional net moisture flux is − 1.09 kg m^{-1} s^{-1}. In the LEOC1050, the net moisture flux decreases to − 2.40 kg m^{-1} s^{-1}, with more moisture being removed from the red rectangle region from the southern and northern boundaries. The net moisture flux decreases from − 0.86 kg m^{-1} s^{-1} in the EEOC560 experiment to − 1.92 kg m^{-1} s^{-1} in the LEOC560 experiment, and from − 3.45 kg m^{-1} s^{-1} in the EE560 experiment to − 5.91 kg m^{-1} s^{-1} in the LE560 experiment (Fig. 2A and B).

The following show how the forcing factors of topography, land–sea redistribution and global cooling induced by atmospheric CO_2 decrease modify the regional moisture flux.

3.2.1. Topography

Under the Early Eocene conditions, the topography leads to a reduction in the net moisture flux by 0.31 kg m^{-1} s^{-1} (EE560 vs. EE560Flat) in the red rectangle (Fig. 4A). Under the Late Eocene

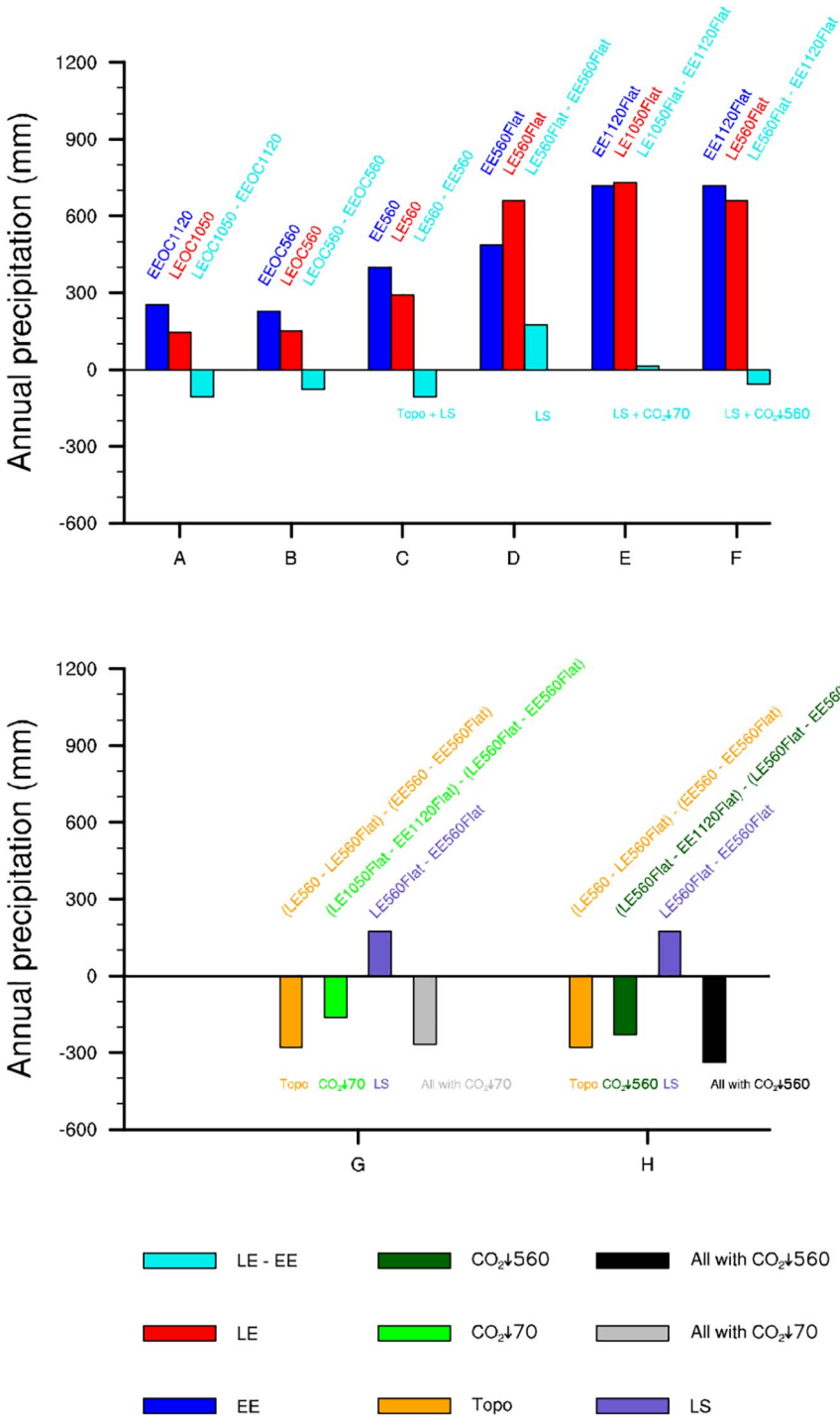

Fig. 3. Annual precipitation (mm) averaged over the focused region of the Asian inland (30°–40° N, 75°–95° E; red box in Fig. 2) for the Early Eocene (EE, blue bar), Late Eocene (LE, dark blue bar), and the anomaly between them (LE – EE, light blue bar, the Late Eocene minus the Early Eocene) (in A, B, C, D, E, and F), and for the climate effect evaluations of the forcing factors (in G and H), with the indicated calculation methods at the top of the bars. Light blue bars in C, D, E, and F represent the effect/combined effects of topography change and land–sea redistribution (Topo + LS), land–sea redistribution (LS), land–sea redistribution and global cooling induced by a 70 ppmv atmospheric CO_2 decrease (LS + CO_2↓70), land–sea redistribution and global cooling induced by a 560 ppmv atmospheric CO_2 decrease (LS + CO_2↓560), respectively. The evaluations of the climate effects of topography change (orange bar, in G and H), global cooling induced by a 70 ppmv atmospheric CO_2 decrease (light green bar, in G), global cooling induced by a 560 ppmv atmospheric CO_2 decrease (dark green bar, in H), land–sea redistribution (purple bar, in G and H), their combined effects with a 70 ppmv atmospheric CO_2 decrease (gray bar, in G), and their combined effects with a 560 ppmv atmospheric CO_2 decrease (black bar, in H) on Asian inland annual precipitation are shown in G and H. (For interpretation of the references to colour in this figure legend, the reader is referred to the web version of this article.)

boundary condition, the elevated higher topography remarkably reduces the net moisture flux by 6.27 kg m^{-1} s^{-1} in experiment LE560 compared with experiment LE560Flat (Fig. 4B). This reduction is related to the weakened westerlies bearing less moisture into the red rectangle and the intensified southerlies removing more moisture from the red rectangle region (Fig. 4B). Moreover, the higher topography in the Late Eocene is beneficial for atmospheric subsidence in the Asian inland, thus limiting rainfall (Fig. 4D). Therefore, the changes in topography, in particular the early uplift of the Tibetan Plateau, have strong impacts on the reduction of Asian inland annual precipitation (Fig. 4A vs. B).

3.2.2. Land–sea redistribution

Due to the changes in land–sea distribution, more moisture is transported into the Asian inland in the Late Eocene experiment relative to that in the Early Eocene experiment. The net moisture flux in the red rectangle region is − 3.14 kg m^{-1} s^{-1} in the EE560Flat (Fig. 2C) but 0.36 kg m^{-1} s^{-1} in the LE560Flat (Fig. 2D). The regional net moisture increases by 3.49 kg m^{-1} s^{-1} (Fig. 5B).

This is related to anomalous westerlies and southerlies due to land–sea redistribution (Fig. 5E). On the one hand, the anomalous south-to-north sea level pressure gradient between tropical Asia and the mid-latitude Asian land in the Late Eocene flat earth experiment LE560Flat induces anomalous southerlies (Fig. 5E), benefiting more moisture from tropics transported northward into the Asian inland

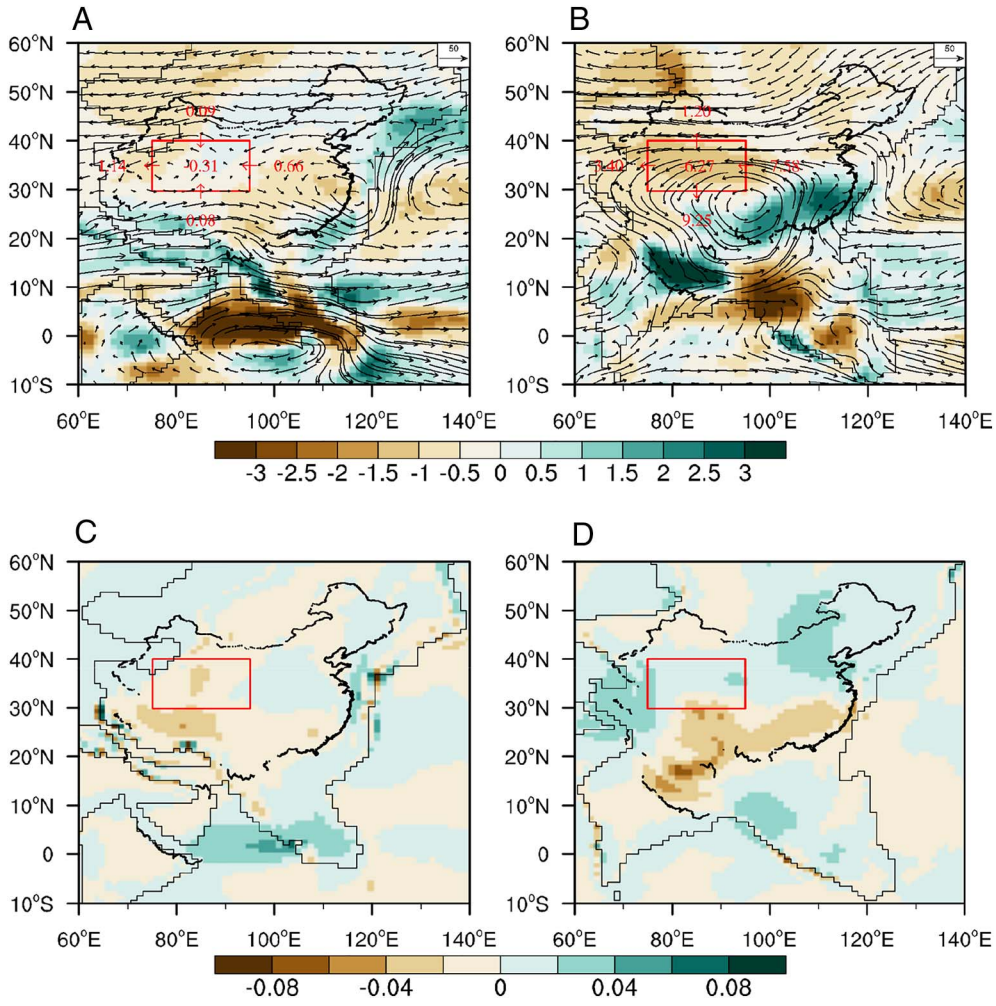

Fig. 4. Impacts of topography in the Early Eocene (left panels, difference between EE560 and EE560Flat) and in the Late Eocene (right panels, difference between LE560 and LE560Flat). Changes in the annual precipitation (A and B, shaded; mm day^{-1}), vertically integrated water vapor flux (A and B, arrow, units: kg m^{-1} s^{-1}), and vertical velocity at 500 hPa (C and D, shaded; units: Pa s^{-1}). The red rectangle outlines the focused region over the Asian inland (30°–40° N, 75°–95° E). (For interpretation of the references to colour in this figure legend, the reader is referred to the web version of this article.)

(Fig. 5B). On the other hand, the meridional temperature gradient over the Asian inland increases in the Late Eocene flat earth experiment LE560Flat (Fig. 5H). The increased meridional temperature gradient benefits stronger westerlies based on thermal wind theory (Fig. 5K). In addition, the atmospheric water content increases slightly due to the Eocene land–sea redistribution (Fig. 5B). The strengthened westerlies transport more moisture across the Asian inland. Thus, the land–sea redistribution results in a regional rainfall increase and does not contribute to the enhanced Eocene aridity in the Asian inland. Consistently, previous sensitive simulations show that the retreat of the Paratethys Sea during the Eocene does not contribute to aridity in Northwest China (see Fig. 6c in Zhang et al., 2007).

3.2.3. Global cooling induced by atmospheric CO_2 decrease

Global cooling induced by atmospheric CO_2 decrease reduces the regional net moisture flux by 1.05 kg m^{-1} s^{-1}. Moisture transported from the west decreases by 0.2 kg m^{-1} s^{-1}. While moisture transported out by northerlies increases by 1.28 kg m^{-1} s^{-1} (Fig. 5C). This global cooling reduces the moisture transported by the westerlies in two ways. First, the CO_2 decrease induces a global temperature decrease and thus results in lowered atmospheric water content (Fig. 5C). Second, the global cooling reduces the meridional temperature gradient over the Asian inland because the magnitude of the troposphere temperature decrease here is larger than the neighboring meridional regions (Fig. 5I). Consequently, the strength of the westerly wind weakens based on thermal wind theory (Fig. 5L). The reduced water content and weakened westerlies lead to a decrease in the moisture transported by the westerlies across the Asian inland. In addition, the anomalous high sea level pressure in the Asian inland causes more moisture to be transported out by the northerlies (Fig. 5F). Therefore, the global cooling induced by atmospheric CO_2 decrease could reduce the regional net moisture flux and precipitation and contribute to enhanced Eocene aridity in the Asian inland.

4. Discussion

4.1. Uncertainties

Our sensitivity experiments show that the effect of topography is larger in the enhanced Eocene Asian inland aridity than the effect of the global cooling caused by decreased atmospheric CO_2 level (Fig. 3G). However, the reconstructions of the atmospheric CO_2 concentration and topography have many uncertainties. These uncertainties may have influenced our conclusion and should be assessed.

The paleoaltitude of the early Tibetan Plateau is still under intense debate. Some geological evidence supports a higher central Tibetan Plateau in the Late Eocene. At that time, the central Tibetan Plateau might have reached present elevation. Lhasa and southern Qiangtang terranes, which formed the proto-Tibetan Plateau, are estimated to have attained their near modern elevation since 40 Ma (Wang et al., 2008). The oxygen-isotope-based estimations of paleoaltitude suggest that the Lunpola Basin was elevated to over 4 km by 39 Ma (Rowley and Currie, 2006). Palynologically derived height analysis suggests that the Gangdise-Nyainqentanglha region was likely higher than 3 km by at least the Late Eocene (Song et al., 2010). However, most of evidence suggests that the central and southern parts of TP elevated during the

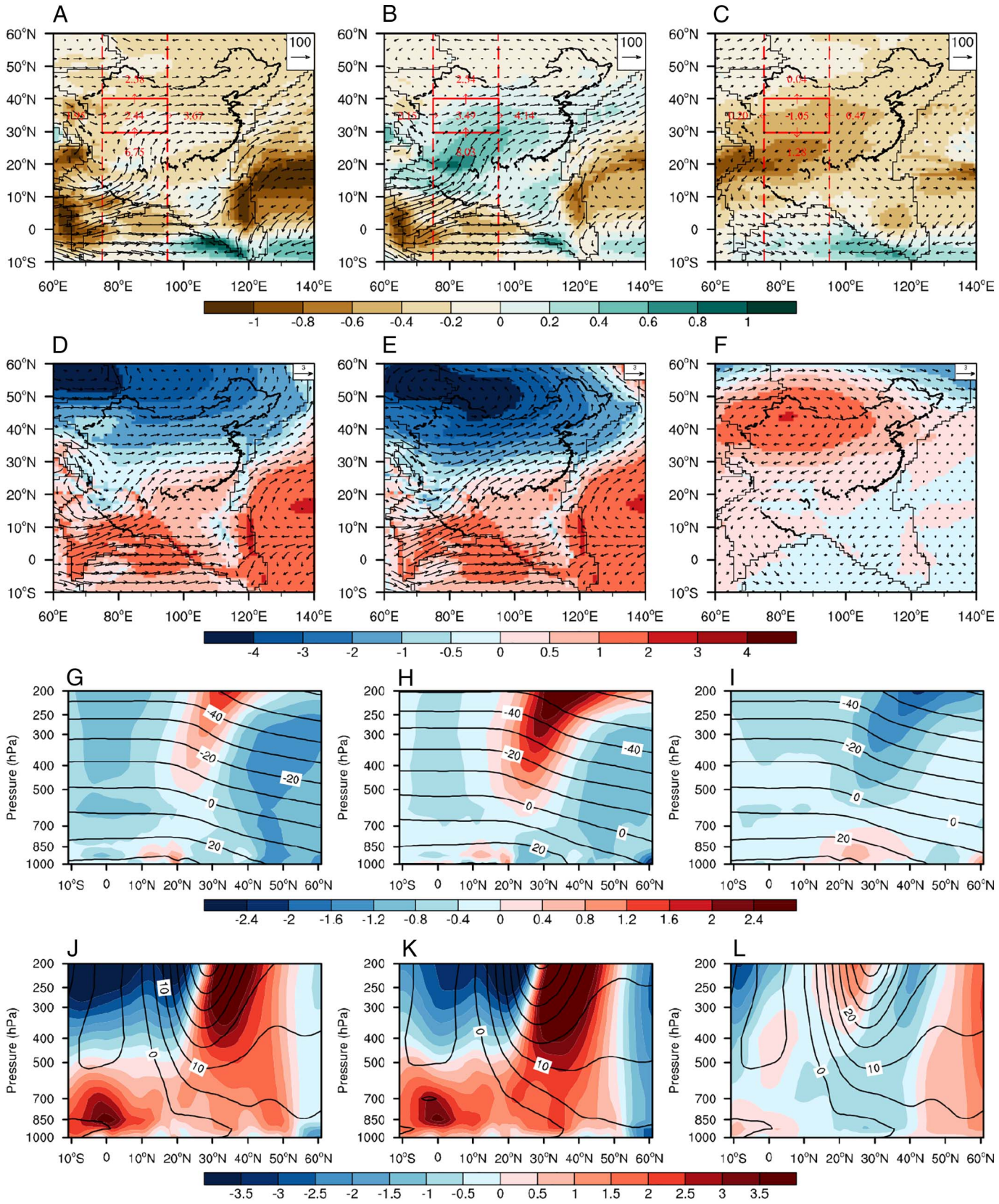

Fig. 5. Impacts of land–sea redistribution (center panels, difference between LE560Flat and EE560Flat), global cooling induced by decrease in atmospheric CO_2 concentrations (right panels, difference between (LE1050Flat − EE1120Flat) and (LE560Flat − EE560Flat)), and their combination (left panels, difference between LE1050Flat and EE1120Flat) on the Asian inland precipitation. Changes in the vertically averaged specific humidity (A, B, and C, shading, units: g kg^{-1}) and vertically integrated water vapor flux (A, B, and C, arrow, units: kg m^{-1} s^{-1}). Changes in the sea level pressure (D, E, and F, shading, units: hPa) and wind at 850 hPa (D, E, and F, arrow, units: m^{-1} s^{-1}). Changes in the temperature (G, H, and I, shading, units: °C) and the zonal wind (J, K, and L, shading, units: m s^{-1}) averaged over 75°–95° E (outlined by red dash lines in A, B, and C). The red rectangles in A, B and C outline the focused region over the Asian inland (30°–40° N, 75°–95° E). The black lines in G and I represent the temperatures in experiment EE1120FLat. The black lines in H represent the temperatures in experiment EE560Flat. The black lines in J and L represent the zonal wind in experiment EE1120Flat. The black lines in K represent the zonal winds in experiment EE560Flat. (For interpretation of the references to colour in this figure legend, the reader is referred to the web version of this article.)

Eocene. The uplift of these parts is the major forcing for the Asian inland aridity, as simulated in the early studies (Figs. 3 and 4 in Zhang et al., 2015).

In our Late Eocene sensitivity experiments, the Tibetan Plateau is approximately 2200–2800 m (see Supplementary Fig. 1), lower than the height estimated by the above geological evidence, although still in agreement with other geological evidence. Due to the low elevation of the Tibetan Plateau, our sensitivity experiments may have underestimated the impact of early Tibetan Plateau uplift on the Asian inland aridity. The diagnosed annual precipitation reduction by 280 mm is close to the lowest value caused by the uplift of the early Tibetan Plateau.

The estimated Eocene atmospheric CO_2 concentrations based on different proxies provide a very wide range. The estimation of the atmospheric CO_2 concentration ranges from 1260 to 680 ppmv in the Early Eocene (51.3–48.9 Ma) based on the nahcolite proxy in evaporite deposits of the Green River Formation, Piceance Creek Basin, Colorado, USA (Jagniecki et al., 2015); from 1000 to 700 ppmv at about 40 Ma based on stomatal indices of fossil *Metasequoia* needles from the Giraffe kimberlite locality in northwestern Canada (Doria et al., 2011); and from 1200 to 700 ppmv from the middle–late Eocene to the early Oligocene (39–28 Ma) based on alkenones in phytoplankton from Ocean Drilling Program Site 925 (Y.G. Zhang et al., 2013). In our experiments, two atmospheric CO_2 levels, 1120 and 560 ppmv, were used that almost cover the entire range of estimated Eocene atmospheric CO_2 concentrations. With the large decrease in atmospheric CO_2 levels to 560 ppmv, the annual precipitation decreases by 231 mm under the Early Eocene boundary condition (EE560Flat − EE1120Flat) and by 70 mm under the Late Eocene boundary condition (LE560-Flat − LE1050Flat). These two values are smaller than the likely underestimated precipitation reduction of 280 mm caused by the early Tibetan Plateau uplift (Fig. 3G). Moreover, our simulations show that decrease in atmospheric CO_2 concentration by itself is insufficient to account for the total Asian inland precipitation reduction. Therefore, our diagnosis suggests that the uplift of the early Tibetan Plateau plays at least as important a role as global cooling induced by decrease in atmospheric CO_2 does on the Asian inland enhanced Eocene aridity.

4.2. Implications for intensified Eocene Asian aridity

Our simulations support the conclusion found from geological evidence that Asian inland aridity was enhanced during the Eocene (Song et al., 2013; Bosboom et al., 2014b; Fang et al., 2015; Miao et al., 2016). Our simulations show that this aridification is caused by changes in topography, in particular the early uplift of the central Tibetan Plateau, and the global cooling induced by decreased atmospheric CO_2 concentration. Our sensitivity experiments suggest that topography change is more important in determining the long-term trend of Asian inland aridification during the Eocene.

However, geological evidence also shows short-term fluctuations in this Eocene Asian inland aridification on hundreds of thousands of years timescale (Song et al., 2013; Fang et al., 2015). Since there is no evidence to indicate that the Tibetan Plateau could build up but collapse again over a few million years, it is implausible to attribute the short-term fluctuations to the Tibetan Plateau uplift. We propose that variation in the atmospheric CO_2 concentration is more important in modulating the regional aridity, leading to the short-term fluctuations in this Eocene Asian inland aridification.

5. Conclusions

In summary, we have simulated the enhanced Asian inland aridity during the Eocene, which is in agreement with geological evidence. Our simulations demonstrate that the simulated aridification is closely related to the deficient regional moisture budget. In additional to the global cooling induced by decrease in the atmospheric CO_2 concentration, as suggested by early studies, our simulations suggest that the early uplift of the Tibetan Plateau also contributed to the long-term Asian inland aridification during the Eocene. The uplift of the early Tibetan Plateau played at least as important a role as the global cooling induced by a decrease in atmospheric CO_2 in enhancing Asian inland aridity during the Eocene.

Acknowledgments

This work was supported by National Natural Science Foundation of China (41472160 and 41775088), the Thousand Talents Program for Distinguished Young Scholars (Zhongshi Zhang), National Natural Science Foundation of China (41402158), and the China Postdoctoral Science Foundation funded project (2015M581154). Xiangyu Li would like to thank Baohuang Su for drawing assistance and Dr. Yibo Yang for valuable discussion.

Appendix A. Supplementary data

Supplementary data to this article can be found online at https://doi.org/10.1016/j.palaeo.2017.10.029.

References

Abels, H.A., Dupont-Nivet, G., Xiao, G., Bosboom, R., Krijgsman, W., 2011. Step-wise change of Asian interior climate preceding the Eocene–Oligocene Transition (EOT). Palaeogeogr. Palaeoclimatol. Palaeoecol. 299, 399–412.

An, Z., Kutzbach, J.E., Prell, W.L., Porter, S.C., 2001. Evolution of Asian monsoons and phased uplift of the Himalaya–Tibetan plateau since Late Miocene times. Nature 411, 62–66.

Bentsen, M., Bethke, I., Debernard, J.B., Iversen, T., Kirkevåg, A., Seland, Ø., Drange, H., Roelandt, C., Seierstad, I.A., Hoose, C., Kristjánsson, J.E., 2013. The Norwegian earth system model, NorESM1-M – part 1: description and basic evaluation of the physical climate. Geosci. Model Dev. 6, 687–720.

Bice, K.L., Barron, E.J., Peterson, W.H., 1998. Reconstruction of realistic Early Eocene paleobathymetry and ocean GCM sensitivity to specified basin configuration. In: Crowley, T., Burke, K. (Eds.), Tectonic Boundary Conditions for Climate Reconstructions. Oxford Univ. Press, pp. 227–247.

Bosboom, R.E., Dupont-Nivet, G., Houben, A.J.P., Brinkhuis, H., Villa, G., Mandic, O., Stoica, M., Zachariasse, W.J., Guo, Z., Li, C., Krijgsman, W., 2011. Late Eocene sea retreat from the Tarim Basin (west China) and concomitant Asian paleoenvironmental change. Palaeogeogr. Palaeoclimatol. Palaeoecol. 299, 385–398.

Bosboom, R., Dupont-Nivet, G., Grothe, A., Brinkhuis, H., Villa, G., Mandic, O., Stoica, M., Huang, W., Yang, W., Guo, Z., Krijgsman, W., 2014a. Linking Tarim Basin sea retreat (west China) and Asian aridification in the late Eocene. Basin Res. 26, 621–640.

Bosboom, R.E., Abels, H.A., Hoorn, C., van den Berg, B.C.J., Guo, Z., Dupont-Nivet, G., 2014b. Aridification in continental Asia after the Middle Eocene Climatic Optimum (MECO). Earth Planet. Sci. Lett. 389, 34–42.

Ding, Z.L., Xiong, S.F., Sun, J.M., Yang, S.L., Gu, Z.Y., Liu, T.S., 1999. Pedostratigraphy and paleomagnetism of a ~7.0 Ma eolian loess–red clay sequence at Lingtai, Loess Plateau, north-central China and the implications for paleomonsoon evolution. Palaeogeogr. Palaeoclimatol. Palaeoecol. 152, 49–66.

Doria, G., Royer, D.L., Wolfe, A.P., Fox, A., Westgate, J.A., Beerling, D.J., 2011. Declining atmospheric CO_2 during the late Middle Eocene climate transition. Am. J. Sci. 311, 63–75.

Dupont-Nivet, G., Krijgsman, W., Langereis, C.G., Abels, H.A., Dai, S., Fang, X., 2007. Tibetan plateau aridification linked to global cooling at the Eocene-Oligocene transition. Nature 445, 635–638.

Fang, X., Xi, X., Li, J., Mu, D., 1997. Late Miocene drying of western China. Chin. Sci. Bull. 42, 2521–2524.

Fang, X., Zan, J., Appel, E., Lu, Y., Song, C., Dai, S., Tuo, S., 2015. An Eocene–Miocene continuous rock magnetic record from the sediments in the Xining Basin, NW China: indication for Cenozoic persistent drying driven by global cooling and Tibetan Plateau uplift. Geophys. J. Int. 201, 78–89.

Fu, Z., Yuan, X., Geng, G., 1994. The Tertiary of the Hetao Basin and its biotas. J. Stratigr. 18, 24–29 (in Chinese with English abstract).

Gent, P.R., Yeager, S.G., Neale, R.B., Levis, S., Bailey, D.A., 2010. Improvements in a half degree atmosphere/land version of the CCSM. Clim. Dyn. 34, 819–833.

Graham, S.A., Chamberlain, C.P., Yue, Y., Ritts, B.D., Hanson, A.D., Horton, T.W., Waldbauer, J.R., Poage, M.A., Feng, X., 2005. Stable isotope records of Cenozoic climate and topography, Tibetan plateau and Tarim basin. Am. J. Sci. 305, 101–118.

Guo, Z.T., Ruddiman, W.F., Hao, Q.Z., Wu, H.B., Qiao, Y.S., Zhu, R.X., Peng, S.Z., Wei, J.J., Yuan, B.Y., Liu, T.S., 2002. Onset of Asian desertification by 22 Myr ago inferred from loess deposits in China. Nature 416, 159–163.

Guo, Z.T., Sun, B., Zhang, Z.S., Peng, S.Z., Xiao, G.Q., Ge, J.Y., Hao, Q.Z., Qiao, Y.S., Liang, M.Y., Liu, J.F., Yin, Q.Z., Wei, J.J., 2008. A major reorganization of Asian climate by the early Miocene. Clim. Past 4, 153–174.

Jagniecki, E.A., Lowenstein, T.K., Jenkins, D.M., Demicco, R.V., 2015. Eocene

atmospheric CO_2 from the nahcolite proxy. Geology 43, 1075–1078.
Jin, X., 1996. Cretaceous-Tertiary micropaleontologic flora and fauna in Turpan-Hami Basin. Pet. Explor. Dev. 23, 33–38 (in Chinese).
Lin, S.-J., 2004. A "vertically Lagrangian" finite-volume dynamical core for global models. Mon. Weather Rev. 132, 2293–2307.
Lin, S.-J., Rood, R.B., 1997. An explicit flux-form semi-lagrangian shallow-water model on the sphere. Q. J. R. Meteorol. Soc. 123, 2477–2498.
Liu, T., 1985. Loess and the Environment. China Ocean Press, Beijing (251 pp.).
Liu, T., Zheng, M., Guo, Z., 1998. Initiation and evolution of the Asian monsoon system timely coupled with the ice-sheet growth and the tectonic movements in Asia. J. Quat. Sci. 3, 194–204 (in Chinese with English abstract).
Miao, Y., Fang, X., Song, Z., Wu, F., Han, W., Dai, S., Song, C., 2008. Late Eocene pollen records and palaeoenvironmental changes in northern Tibetan Plateau. Sci. China Ser. D Earth Sci. 51, 1089–1098.
Miao, Y., Wu, F., Chang, H., Fang, X., Deng, T., Sun, J., Jin, C., 2016. A Late-Eocene palynological record from the Hoh Xil Basin, northern Tibetan Plateau, and its implications for stratigraphic age, paleoclimate and paleoelevation. Gondwana Res. 31, 241–252.
Mulch, A., Chamberlain, C.P., 2006. Earth science: the rise and growth of Tibet. Nature 439, 670–671.
Neale, R.B., Richter, J., Park, S., Lauritzen, P.H., Vavrus, S.J., Rasch, P.J., Zhang, M., 2013. The mean climate of the Community Atmosphere Model (CAM4) in forced SST and fully coupled experiments. J. Clim. 26, 5150–5168.
Polissar, P.J., Freeman, K.H., Rowley, D.B., McInerney, F.A., Currie, B.S., 2009. Paleoaltimetry of the Tibetan Plateau from D/H ratios of lipid biomarkers. Earth Planet. Sci. Lett. 287, 64–76.
Qiang, X., An, Z., Song, Y., Chang, H., Sun, Y., Liu, W., Ao, H., Dong, J., Fu, C., Wu, F., Lu, F., Cai, Y., Zhou, W., Cao, J., Xu, X., Ai, L., 2011. New eolian red clay sequence on the western Chinese Loess Plateau linked to onset of Asian desertification about 25 Ma ago. Sci. China Earth Sci. 54, 136–144.
Rea, D.K., Snoeckx, H., Joseph, L.H., 1998. Late Cenozoic eolian deposition in the North Pacific: Asian drying, Tibetan uplift, and cooling of the northern hemisphere. Paleoceanography 13, 215–224.
Rowley, D.B., Currie, B.S., 2006. Palaeo-altimetry of the late Eocene to Miocene Lunpola basin, central Tibet. Nature 439, 677–681.
Ruddiman, W.F., Kutzbach, J.E., 1991. Plateau uplift and climatic change. Sci. Am. 264, 66–72.
Scotese, C.R., 2001. Digital Paleogeographic Map Archive on CD-ROM, PALEOMAP Project, Arlington, Texas.
Song, X.-Y., Spicer, R.A., Yang, J., Yao, Y.-F., Li, C.-S., 2010. Pollen evidence for an Eocene to Miocene elevation of central southern Tibet predating the rise of the High Himalaya. Palaeogeogr. Palaeoclimatol. Palaeoecol. 297, 159–168.
Song, B., Zhang, K., Lu, J., Wang, C., Xu, Y., 2013. The middle Eocene to early Miocene integrated sedimentary record in the Qaidam Basin and its implications for paleoclimate and early Tibetan Plateau uplift. Can. J. Earth Sci. 50, 183–196.
Sun, X., Wang, P., 2005. How old is the Asian monsoon system?—Palaeobotanical records from China. Palaeogeogr. Palaeoclimatol. Palaeoecol. 222, 181–222.
Sun, J., Windley, B.F., 2015. Onset of aridification by 34 Ma across the Eocene-Oligocene transition in Central Asia. Geology 43, 1015–1018.
Sun, D., Shaw, J., An, Z., Cheng, M., Yue, L., 1998. Magnetostratigraphy and paleoclimatic interpretation of a continuous 7.2 Ma Late Cenozoic Eolian sediments from the Chinese Loess Plateau. Geophys. Res. Lett. 25, 85–88.
Sun, J., Ye, J., Wu, W., Ni, X., Bi, S., Zhang, Z., Liu, W., Meng, J., 2010. Late Oligocene–Miocene mid-latitude aridification and wind patterns in the Asian interior. Geology 38, 515–518.
Sun, Y., Ma, L., Bloemendal, J., Clemens, S., Qiang, X., An, Z., 2015. Miocene climate change on the Chinese Loess Plateau: possible links to the growth of the northern Tibetan Plateau and global cooling. Geochem. Geophys. Geosyst. 16, 2097–2108.
Tang, Z., Ding, Z., White, P.D., Dong, X., Ji, J., Jiang, H., Luo, P., Wang, X., 2011. Late Cenozoic central Asian drying inferred from a palynological record from the northern Tian Shan. Earth Planet. Sci. Lett. 302, 439–447.
Wang, C., Zhao, X., Liu, Z., Lippert, P.C., Graham, S.A., Coe, R.S., Yi, H., Zhu, L., Liu, S., Li, Y., 2008. Constraints on the early uplift history of the Tibetan Plateau. Proc. Natl. Acad. Sci. U. S. A. 105, 4987–4992.
Zhang, Z., Huijun, W., Zhengtang, G., Dabang, J., 2007. What triggers the transition of palaeoenvironmental patterns in China, the Tibetan Plateau uplift or the Paratethys Sea retreat? Palaeogeogr. Palaeoclimatol. Palaeoecol. 245, 317–331.
Zhang, Z., Nisancioglu, K.H., Flatøy, F., Bentsen, M., Bethke, I., Wang, H., 2011. Tropical seaways played a more important role than high latitude seaways in Cenozoic cooling. Clim. Past 7, 801–813.
Zhang, R., Jiang, D., Liu, X., Tian, Z., 2012. Modeling the climate effects of different subregional uplifts within the Himalaya-Tibetan Plateau on Asian summer monsoon evolution. Chin. Sci. Bull. 57, 4617–4626.
Zhang, Z.S., Nisancioglu, K., Bentsen, M., Tjiputra, J., Bethke, I., Yan, Q., Risebrobakken, B., Andersson, C., Jansen, E., 2012. Pre-industrial and mid-Pliocene simulations with NorESM-L. Geosci. Model Dev. 5, 523–533.
Zhang, Y.G., Pagani, M., Liu, Z., Bohaty, S.M., DeConto, R., 2013. A 40-million-year history of atmospheric CO_2. Phil. Trans. R. Soc. A 371. http://dx.doi.org/10.1098/rsta.2013.0096.
Zhang, Z., Nisancioglu, K.H., Ninnemann, U.S., 2013. Increased ventilation of Antarctic deep water during the warm mid-Pliocene. Nat. Commun. 4, 1499.
Zhang, Y., Sun, D., Li, Z., Wang, F., Wang, X., Li, B., Guo, F., Wu, S., 2014. Cenozoic record of aeolian sediment accumulation and aridification from Lanzhou, China, driven by Tibetan Plateau uplift and global climate. Glob. Planet. Chang. 120, 1–15.
Zhang, Z., Ramstein, G., Schuster, M., Li, C., Contoux, C., Yan, Q., 2014. Aridification of the Sahara desert caused by Tethys Sea shrinkage during the Late Miocene. Nature 513, 401–404.
Zhang, R., Jiang, D., Zhang, Z., Yu, E., 2015. The impact of regional uplift of the Tibetan Plateau on the Asian monsoon climate. Palaeogeogr. Palaeoclimatol. Palaeoecol. 417, 137–150.
Zheng, H., Wei, X., Tada, R., Clift, P.D., Wang, B., Jourdan, F., Wang, P., He, M., 2015. Late Oligocene–early Miocene birth of the Taklimakan Desert. Proc. Natl. Acad. Sci. U. S. A. 112, 7662–7667.
Zhuang, G., Hourigan, J.K., Koch, P.L., Ritts, B.D., Kent-Corson, M.L., 2011. Isotopic constraints on intensified aridity in Central Asia around 12 Ma. Earth Planet. Sci. Lett. 312, 152–163.